Tuning the electronic properties of graphene–graphitic carbon nitride heterostructures and heterojunctions by using an electric field

A. Bafekry [1,*] and M. Neek-Amal [2,†]

[1]*Department of physics, University of Guilan, 41335-1914 Rasht, Iran*
and Department of Physics, University of Antwerp, Groenenborgerlaan 171, B-2020 Antwerp, Belgium
[2]*Department of Physics, Shahid Rajaee University, 16875-163 Lavizan, Tehran, Iran*

(Received 4 November 2019; revised manuscript received 7 January 2020; accepted 31 January 2020; published 24 February 2020)

Integration of graphene-based two-dimensional materials is essential for nanoelectronics applications. Using density-functional theory, we systematically investigate the electronic properties of vertically stacked graphene-graphitic carbon nitrides (GE/GCN). We also studied the covalently lateral stitched graphene-graphitic carbon nitrides (GE-GCN heterojunctions). The effects of perpendicular electric field on the electronic properties of six different heterostructures, i.e., (i) one layer of GE on top of a layer of C_nN_m with $(n, m) = (3, 1)$, (3,4), and (4,3) and (ii) three heterostructures $C_nN_m/C_{n'}N_{m'}$, where $(n, m) \neq (n', m')$ are elucidated. The most important calculated features are (i) the systems GE/C_3N_4, C_3N/C_3N_4, GE-C_3N, GE-C_4N_3, and C_3N-C_3N_4 exhibit semiconducting characteristics having small band gaps of $\Delta_0 = 20$, 250, 100, 100, 80 meV, respectively while (ii) the systems GE/C_4N_3, C_3N/C_4N_3, and C_3N-C_4N_3 show ferromagnetic-metallic properties. In particular, we found that, in semiconducting heterostructures, the band gap increases nontrivially with increasing the absolute value of the applied perpendicular electric field. This work is useful for designing heterojunctions and heterostructures made of graphene and other two-dimensional materials such as those proposed in recent experiments [X. Liu and M. C. Hersam Sci. Adv. **5**, 6444 (2019)].

DOI: 10.1103/PhysRevB.101.085417

I. INTRODUCTION

Two-dimensional graphitic carbon nitrides (2D-GCNs) reveal unusual properties and provide potential applications in photocatalysis, heterogeneous catalysis, and fuel cells [1,2]. For example, polyaniline (C_3N) has been fabricated [3] and exhibits amazing electronic and mechanical properties [4,5]. Also, C_3N_4 as a potential photocatalyst for water splitting [6,7] has electronic and magnetic properties which are drastically modified by injecting a hole by substituting an N atom with a C atom. Also, the C_4N_3 was successfully synthesized [8] and it was identified that it is a half metal [9]. On the other hand, the van der Waals (vdW) heterostructures (HTSs) such as graphene/MoS_2 [7,10–12], graphene/hexagonal boron nitride (GE/h-BN) [13–15], graphene/silicene [16,17], graphene/g-C_3N_4 [18], and graphene/phosphorene [19] have been widely studied experimentally and theoretically. They can preserve the intrinsic electronic properties of the dissimilar two-dimensional material (2DM) and create particularly advantageous electronic properties. Recently, a HTS made of graphene (GE) and 2D-GCN (GE/C_3N) was proposed by Wang *et al.* [20]. The proposed C_3N/graphene exhibits a metallic behavior and is stable under the applied large strains of about 10%. Recently, the lateral and vertical integration of borophene with GE was reported [1]. It was found that boron intercalation under GE results in rotationally commensurate vertical HTSs. Moreover, the fabricated red phosphorus GCN (EPh-GCN) HTS supercapacitor by Ansari *et al.* [21] displays a high capacitance of 465 F/g and excellent cyclic stability. The photocatalyitic behavior of RPh-GCN HTSs was found to be due to narrow band-gap energy, capacitive behavior, and high nitrogen content. Moreover, using *ab initio* simulations, it was found that the metal-free half-metallic behavior in C_4N_3 can be preserved when it is put on a hexagonal boron nitride (h-BN) layer [22].

Although 2DMs hold great potential for a wide range of applications, it is necessary to modulate their intrinsic properties. In the past few years, several approaches have been developed to modify the electronic properties of 2DMs, such as substitutional doping, defect engineering, surface functionalization by adatoms, applying electric field, and strain engineering [23–34].

Here, we report on the integration of GCNs with graphene. Using *ab initio* calculations, we studied the electronic properties of six HTSs and six heterojunctions (HTJs) made of graphene and GCNs. The difference between the lattice parameter of GE and a typical 2D-GCN is smaller than 4%. Therefore, *ab initio* modeling and simulations on these systems become feasible. The effects of perpendicular electric field on the electronic structure and band gap of HTSs are explored. The results show a wide variety of responses of HTSs to the electric field which are different from isolated GCN and emerging unique properties. In particular, in the studied semiconducting HTSs (GE/C_nN_m), the band gap increases nontrivially with increasing the absolute value of applied perpendicular electric field. Furthermore, by analyzing charge distribution along the contact lines of HTJs, we discovered

*Bafekry.asad@gmail.com
†Corresponding author: mehdi.neekamal@gmail.com

TABLE I. Calculated lattice constant and electronic structure of GE, C_3N, C_3N_4, and C_4N_3 monolayers.

Monolayer	Lattice constant(Å)	Electronic structure	Magnetic moment (μ_B)	Gap (eV)
GE	2.46	Semimetal (SM)	0	0
C_3N	4.86	Semiconductor (SC)	0	0.4
C_3N_4	4.74	Semiconductor (SC)	0	1.45
C_4N_3	4.81	Half-metal (HM)	1.0	2.21

that the HTJ made of GE and C_3N has the minimal mismatch at the contact line. This work explores underlying physics of functional materials (HTSs and HTJs) and corresponding band-gap engineering using external uniform electric field.

II. COMPUTATIONAL METHOD

First-principles calculations of energy and electronic structure are performed within the Perdew-Burke-Ernzerhof variant of the generalized gradient approximation [35] method as implemented in OPENMX package [36]. We used norm-conserving pseudopotentials [37] for carbon and nitrogen atoms. The wave functions are expanded by the linear combination of multiple pseudoatomic orbitals generated using a confinement scheme [36,38]. The $\boldsymbol{k}$ points for sampling over the Brillouin zone (BZ) integration were generated using the Monkhorst-Pack scheme [39]. After the convergence tests, we chose the cutoff 350 Ry for GE, C_3N, C_3N, and C_3N_4 monolayers. The latter causes the total energy to be converged below 1.0 meV/atom. For all the studied HTSs and HTJs, we used a cutoff energy of 400 Ry. The geometries were fully relaxed until the force acting on each atom was less than 1 meV/Å. With these parameters, the resulting structures are found to be sufficiently relaxed to obtain well-converged various properties in the next steps of the calculations. The BZ is sampled by a **k**-mesh grid of $23 \times 23 \times 1$ for primitive unit cell of monolayers and for different HTSs and HTJs, we used a **k**-mesh grid of $15 \times 15 \times 1$. In addition, the $\boldsymbol{k}$-mesh includes the high-symmetry points (Γ, M, K) relevant to the hexagonal geometry. The grids of density of states (DOS) and partial density of states (PDOS) calculations are two times denser than that of for the self-consistent calculations. We also used Gaussian smearing width 0.2 eV for the DOS and PDOS calculations. The 2D-GCNs are modeled as a periodic slab with a sufficiently large vacuum layer (20 Å) to avoid interaction between adjacent layers. To accurately describe the vdW interaction between layers of HTSs, we adopted the empirical correction method presented by Grimme (DFT-D2) [40], which is a reliable choice for describing the vdW interactions. To find the minimum energy configurations, we compared various AA with other AA and/or AB stacking for any given HTS.

III. GRAPHENE-GRAPHITIC CARBON NITRIDE HETEROSTRUCTURES (GE/C_nN_m)

We reviewed the geometrical and electronic properties of monolayers of GE, C_3N, C_3N_4, and C_4N_3 in the Supplemental Material [41] (see Figs. S1 and S2 in Supplemental Material Sec. SI). Our results show that (i) C_3N is an indirect semiconductor with 0.4 eV band gap, (ii) C_3N_4 is a direct semiconductor with a band gap of 1.45 eV, (iii) C_4N_3 exhibits half metallicity with a magnetic moment of 1 μ_B per 1×1 unit cell, and (iV) GE is a semimetal with zero gap (see Supplemental Material Sec. SII). The obtained magnetic moment for monolayer C_4N_3 is equal to that reported by Du *et al.* [9]. We listed the lattice constant and other electronic and magnetic properties of the above-mentioned monolayers in Table I.

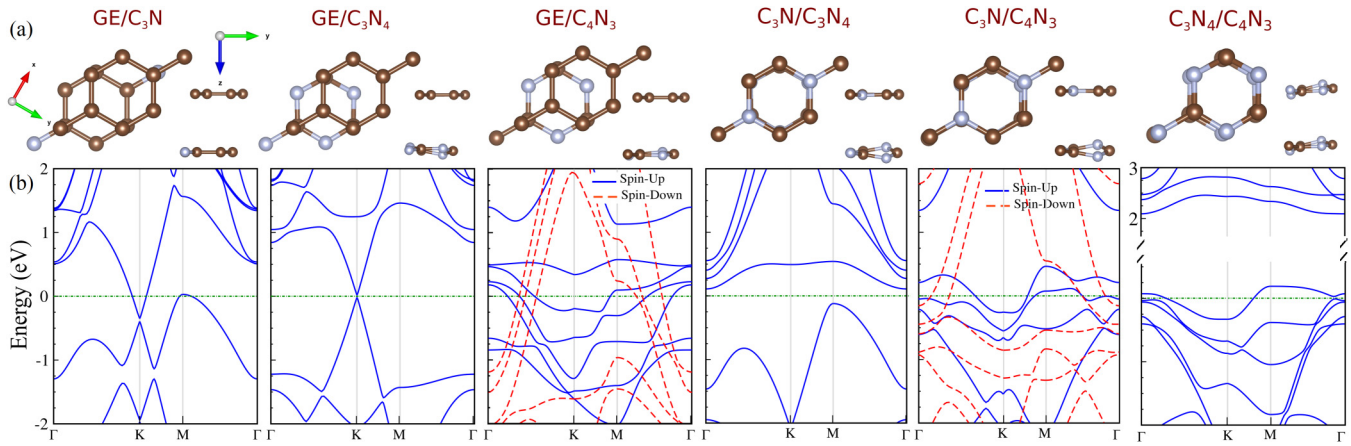

FIG. 1. (a) The most stable heterostructures and (b) the corresponding electronic band structures of GE/C_3N, GE/C_3N_4, GE/C_4N_3, C_3N_4/C_3N, C_4N_3/C_3N, and C_3N_4/C_4N_3 heterostructures. The brown atoms represent C and the blue atoms represent N. The zero energy is set at Fermi level.

TABLE II. The structural, electronic, and magnetic parameters of studied HTSs including lattice constant a, bond length between C-C atoms (d_{CC}), the bond length between N-C atoms (d_{NC}), the optimum interlayer distance between two layers (z_{eq}), the buckling (δ) (i.e., the difference between the largest and smallest z coordinates of C or N atoms in two layers) and the moiré period (L) in Å. The transition of the electronic state (TS) when two individual monolayers are placed on top of each other to form the corresponding HTS was indicated by an arrow ($\rightarrow$) and transition state of HTS in the presence of an electric field of about $E = 0.2V$ Å was indicated by two arrows ($\Rightarrow$). The numbers outside (inside) the parenthesis is for the top (bottom) layer and the magnetic moment per unit cell is listed in the last column. The electronic states are specified as metal (M), ferromagnetic- metal (FM), half- metal (HM), and semiconductor (SC). The band gap of the HTSs (Δ) are also presented when $E = 0$ and $E = 0.2$VÅ.

HTS	a(Å)	d_{CC}(Å)	d_{NC}(Å)	z_{eq}(Å)	δ(Å)	TS ($E = 0$)	Δ (meV)	TS ($E = 0.2$V/Å)	M_{tot}	L(Å)
GE/C_3N	4.92	1.41 (1.41)	– (1.42)	3.47	0 (0)	(SM,SC) $\rightarrow$ M	–	M $\Rightarrow$ M	0	398
GE/C_3N_4	4.88	1.41 (–)	– (1.34)	3.35	0 (0.36)	(SM,SC) $\rightarrow$ SC	20	*SC* $\Rightarrow$ SC	0	129
GE/C_4N_3	4.89	1.41 (1.46)	– (1.36)	3.44	0 (0.17)	(SM,HM) $\rightarrow$ FM	–	–	6.85	215
C_3N/C_3N_4	4.84	1.39 (–)	1.39 (1.48,1.33)	3.36	0 (0.41)	(SC,SC) $\rightarrow$ SC	250	SC $\Rightarrow$ SC	0	191
C_3N/C_4N_3	4.85	1.40 (1.45)	1.39 (1.34)	3.30	0 (0.33)	(SC,HM) $\rightarrow$ FM	–	–	1.4	467
C_3N_4/C_4N_3	4.82	– (1.44)	1.34 (1.35)	3.50	0.36 (0.41)	(SC,HM) $\rightarrow$ M	–	–	0	325

The optimized monolayers of these systems are then used to make the corresponding HTSs and HTJs.

A. The lattice structure of GE/C_nN_m

A 2×2 supercell of graphene and a unit cell of C_3N, C_3N_4, and C_4N_3 are placed on top of each other to form six HTSs, which are shown in Fig. 1(a). The lattice mismatch (λ) between top and bottom layer is defined as

$$\lambda = \frac{|a_T - a_B|}{a_B} \times 100\%, \tag{1}$$

where a_T and a_B are the lattice constants of bottom (C_nN_m) and top layers, respectively. The optimized atomic structure (most stable configurations) of the studied HTSs are shown in Fig. 1(a). After optimization of single layers of GE and C_nN_ms, the lattice mismatch between C_3N, C_3N_4, C_4N_3, and GE are found to be 1.22%, 3.66%, and 2.23%, respectively. Therefore, there is small distortion in the geometrical structure of these systems. The latter enabled us to perform extensive *ab initio* calculations on the HTSs (see the Supplemental Material Fig. S5 for the size effects). Because of the nonzero λ, a moiré pattern appears even when GE and C_nN_m layers are not misaligned. The moiré period (L) is given by [42]

$$L = \frac{a_T}{\sqrt{2(1-\lambda)+\lambda^2}}. \tag{2}$$

The moiré period for all studied HTS are listed in the last column of Table II. It is seen that for all HTSs (except for GE/C_3N_4 where $L = 129$ Å), the moiré period is larger than e.g., the moiré period of GE/h-BN, i.e., 130 Å [42].

The most stable configurations of GE/C_3N, GE/C_3N_4, and GE/C_4N_3 are found to have AB stacking while C_3N_4/C_3N, C_4N_3/C_3N, and C_3N_4/C_4N_4 have AA-stacking arrangements [see Fig. 1(a)]. The obtained parameters for the lattice constant (a), interlayer distance (z_{eq}), and other physical parameters of the HTSs are listed in Table II.

The other possible stackings are shown in Fig. 2. AA and AB refer to the AB stacking and AA stacking. The colored pictures are the most stable HTSs relevant to Fig. 1(a). The ground-state energy (E_0) per area of unit cell for each HTS with respect to the most stable one ($E_n = E - E_0$) is shown in each panel of Fig. 2. Notice that the the most stable HTSs have lower energy (of about 20–70 meV) than the others.

B. Electronic structure of GE/C_nN_m

The electronic band structure and corresponding DOS and PDOS of six studied HTSs are shown in Figs. 1(b) and 3, respectively.

The GE/C_3N exhibit metallic characteristics. In comparison to the pristine graphene, the Dirac point shifts below the Fermi level with energy E_F about 0.5 eV and is located at the K point. Density of states and PDOS of HTSs are shown in Fig. 3. It is seen that at Fermi level of GE/C_3N, the N/C-p_z orbitals of C_3N plays the main role in the electronic state, resulting in the metallic behavior.

Interestingly, the system GE/C_3N_4 is semiconductor with narrow band gap of about 20 meV, where the valence band maximum (VBM) and conduction band minimum (CBM) are located at the K point. Moreover, the VBM and CBM of GE/C_3N_4 are originated from N-p_z and C-p_z orbitals and the N/C-p_z orbitals of C_3N_4, respectively.

The electronic structure of GE/C_4N_3 reveals a ferromagnetic-metal state where the energy bands are split into $\uparrow$ and $\downarrow$ spin channels. The induced magnetic moment into this system is about 6.85 μ_B. Note that the magnetic moment of a single layer of C_4N_3 in a 1-unit cell is $1\mu_B$ (see Table I and Supplemental Material SI). Because of the nonzero magnetic moment of bilayer GE/C_4N_3 and monolayer C_4N_3, we conclude that the magnetism nature of C_4N_3 is preserved when GE/C_4N_3 bilayer is made. For GE/C_4N_3, the states around E_F mainly originate from C-p_z in both $\uparrow$ and $\downarrow$ spin channels and from the N-$p_{x,y}$ of C_4N_3 in the $\uparrow$ spin channel. The degeneracy of both spin channels are broken, which results in a magnetic moment of about 6.85 μ_B per unit cell with 2×2 supercell of graphene and a unit cell of C_4N_3.

The electronic structure results of the above three HTSs show that the electronic structure of GE is preserved for GE/C_3N_4, i.e., a linear band structure appears similar to GE. The same effects (minimal change in the band structure) happens when a GE layer is put on top of a h-BN layer [41,43]. However, for the other HTSs, there is a remarkable

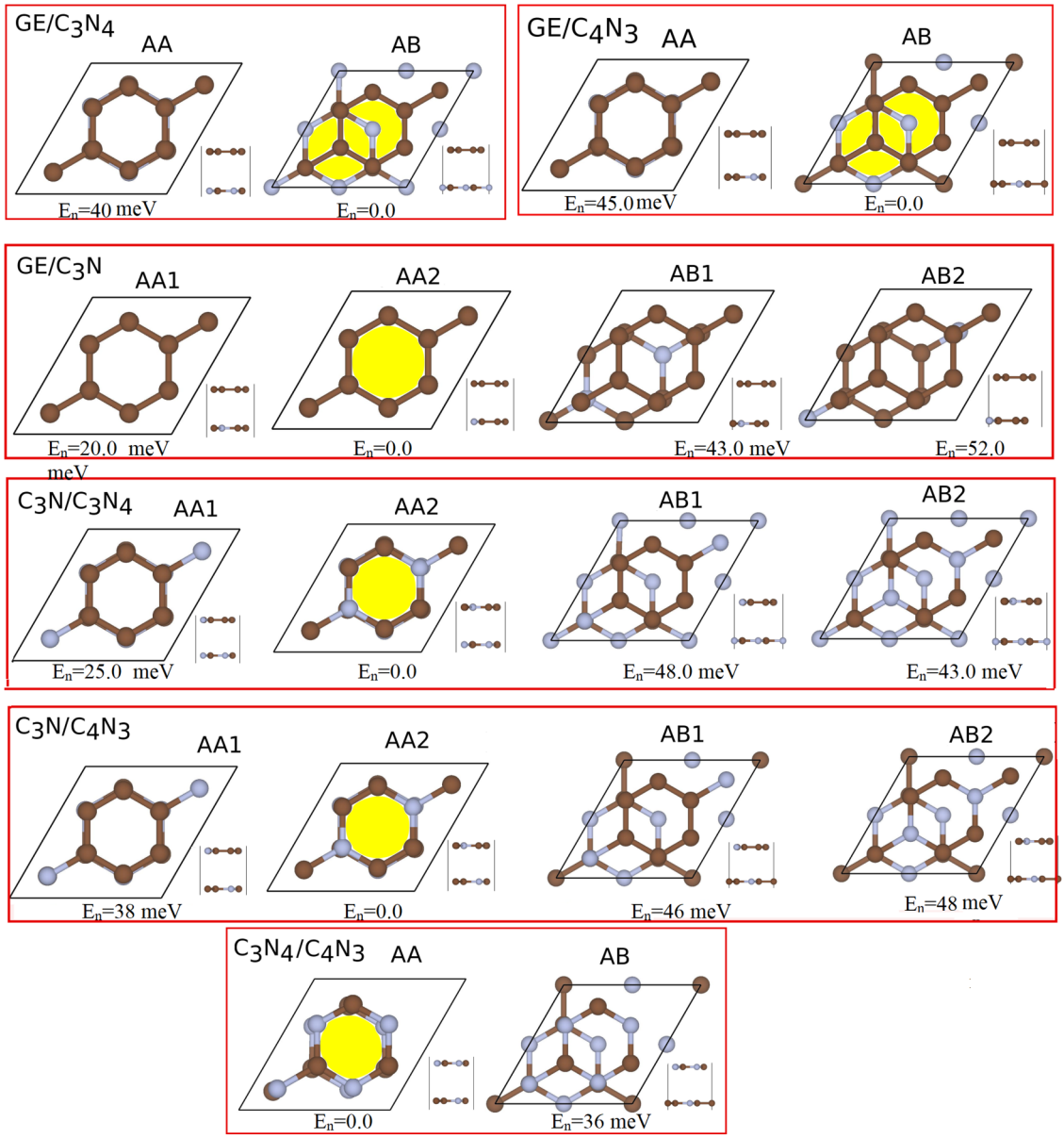

FIG. 2. (Color online.) Schematic illustrations of top and side views for possible stacking of the studied HTSs. The colored pictures are the most stable configurations, where the ground state energy was set to zero, i.e., $E_0 = 0.0$ [see Fig. 1(a)]. Energy per unit cell ($E_n = E - E_0$) is given in bottom of each panel.

difference. [44,45]. However, for the other HTSs, there is a remarkable difference between the HTS and two corresponding monolayers.

C. Electronic structure of $C_nN_m/C_{n'}N_{m'}$

The C_3N/C_3N_4 is an indirect semiconductor having a band gap of 250 meV where the VBM and CBM are located at M and Γ points, respectively. The VBM of GE/C_3N is due to the hybridization of the N-p_z orbitals, while the CBM is formed by the hybridization of C-p_z.

The system C_3N/C_4N_3 is a ferromagnetic metal and has a magnetic moment of 1.4 μ_B, which is due to the magnetic properties of C_4N_3. From DOS and PDOS, we see that VBM of C_3N/C_3N_4 is due to the hybridization of N/C-p_z orbitals of C_3N, while the CBM is due to the hybridization of C-p_z orbitals of C_3N_4.

We found that the system C_3N_4/C_4N_3 reveals metallic features. Interestingly, the magnetic properties of C_4N_3 is eliminated when it makes a HTS with C_3N_4. This may be due to the AA-stacking form of C_3N_4/C_4N_3 which results in symmetry of spin-up and spin-down bands. The magnetic properties (asymmetry in spin-up and spin-down channels) of monolayer C_4N_3 is mainly due to the asymmetry in $N - p_{xy}$ orbitals (either for C atom or in N). But the C_3N_4/C_4N_3 band structure shows that most dominant orbitals are p_z. On the other hand, because the vdW interaction between two layers can be affected by this p_z orbitals, we expect to see larger effects in the electronic structure of C_3N_4/C_4N_3 resulting from pz orbitals which are symmetric

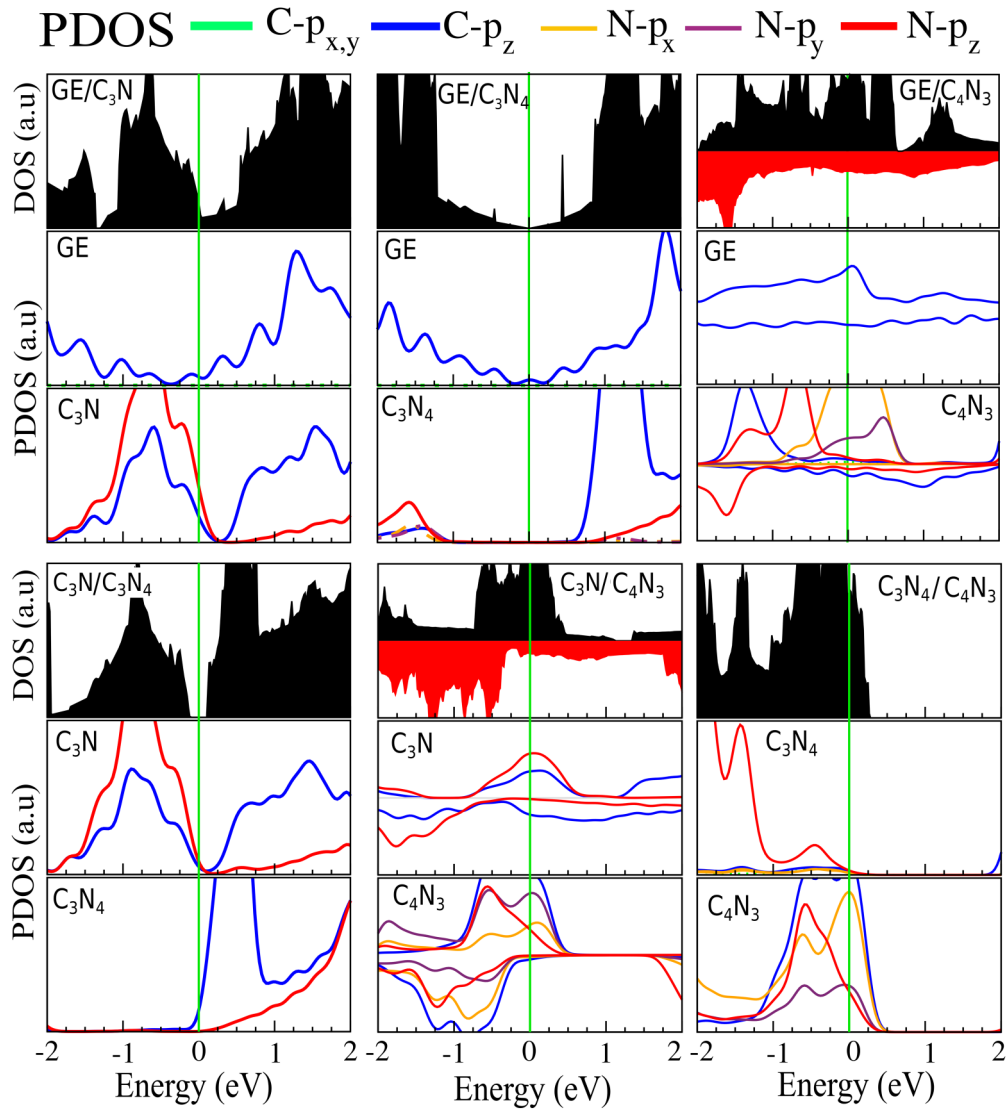

FIG. 3. Density of states and partial density of states of GE/C_3N, GE/C_3N_4, GE/C_4N_3, C_3N_4/C_3N, C_4N_3/C_3N, and C_3N_4/C_4N_3 heterostructures. The zero energy is set at Fermi level.

in C_4N_3 and C_3N_4 monolayers as well as C_3N_4/C_4N_3 bilayer.

Our results for C_3N/C_4N_3 show that the states around E_F mainly originate from the N-p_z of C_3N and the N-$p_{x,y}$ of C_4N_3. Moreover, in C_3N_4/C_4N_3, the state at E_F belongs to the N-$p_{x,y}$ and C-p_z orbitals of C_4N_3 yielding the metallic

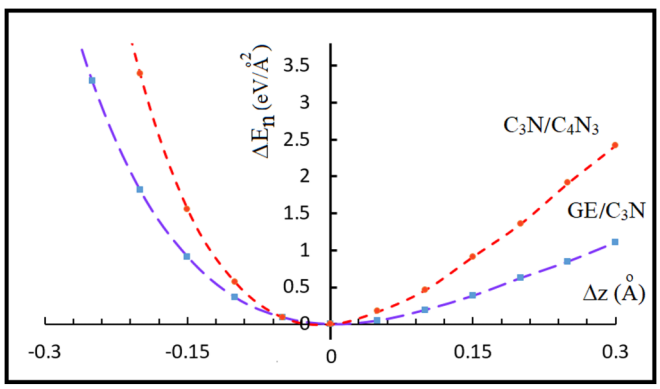

FIG. 4. The relative binding energy with respect to interlayer distance of GE/C_3N and C_3N/C_4N_3 HTSs.

TABLE III. The lattice constants a and b, the magnetic moment per unit cell (M_{tot}), and the electronic state of the studied heterojunctions. Different electronic states are labeled as Dirac semi-metal (DSM), half metal (HM), semimetal (SM), ferromagnetic metal (FM), and semiconductor (SC). The band gap Δ of the systems are shown in the third column listed. The transition of the electronic state (TS) when two individual monolayers are connected laterally to form the corresponding HTJ is indicated by an arrow (→).

HTJ	a(Å)	b(Å)	TS	Δ (meV)	M_{tot}
GE-C_3N	19.58	4.92	(SM,SC) → SC	100 meV	0
GE-C_3N_4	19.59	4.89	(SM,SC) → DSM	–	0
GE-C_4N_3	19.62	4.90	(SM,HM) → SC	100 meV	0
C_3N-C_3N_4	19.48	4.87	(SC,SC) → SC	80 meV	0
C_3N-C_4N_3	19.52	4.88	(SC,HM) → FM	–	1.7
C_3N_4-C_4N_3	19.31	4.82	(SM,HM) → HM	–	4

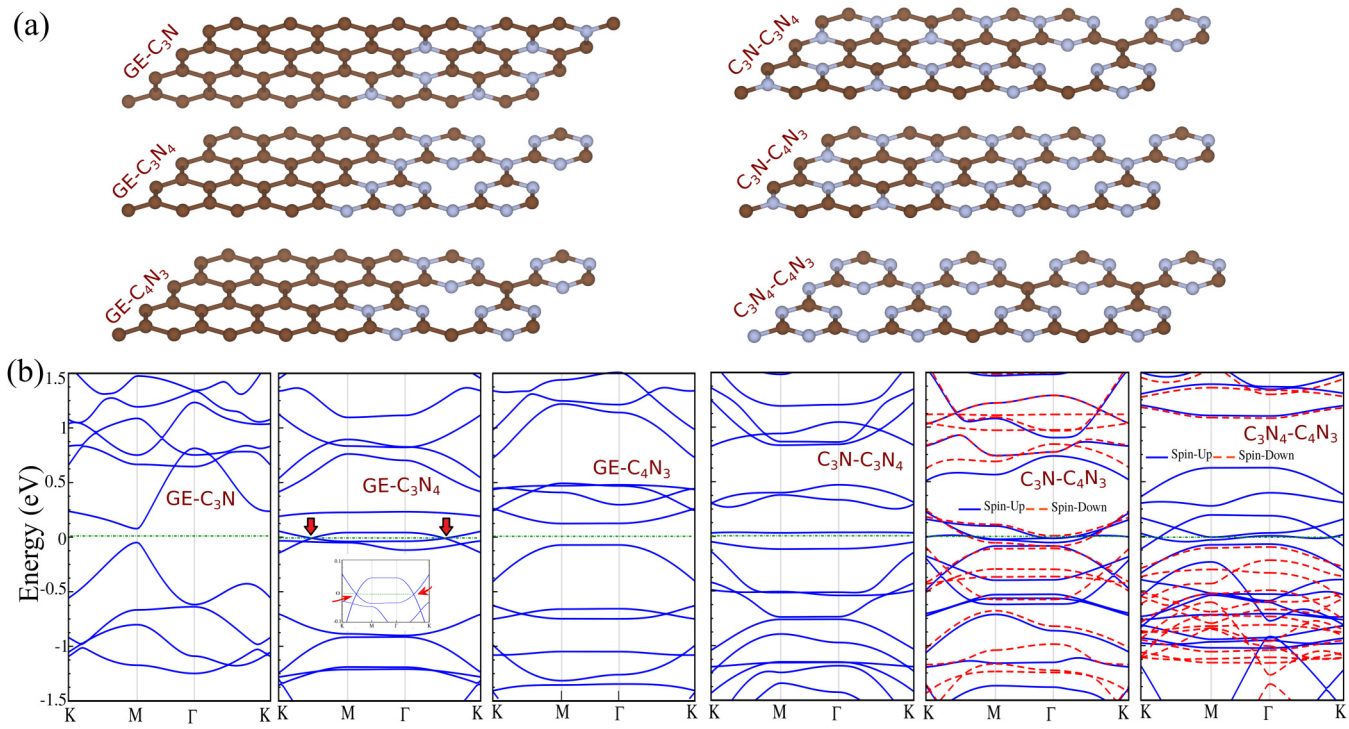

FIG. 5. (a) The optimized atomic structures and the corresponding (b) electronic band structure of GE-C_3N, GE-C_3N_4, GE-C_4N_3, C_3N_4-C_3N, C_4N_3-C_3N, and C_3N_4-C_4N_3 heterojunctions. The brown atoms represent C and the blue atoms represent N. The zero of energy is set at Fermi level. Two Dirac-like points corresponding to the nodal line feature of GE-C_3N_4 are shown in the inset and by red arrows.

character. Notice that the initial magnetic feature of C_4N_3 is lost when it is put over C_3N_4.

To show clearly the changes in the electronic band structure of the monolayers when they make HTS, in Fig. S4 of the

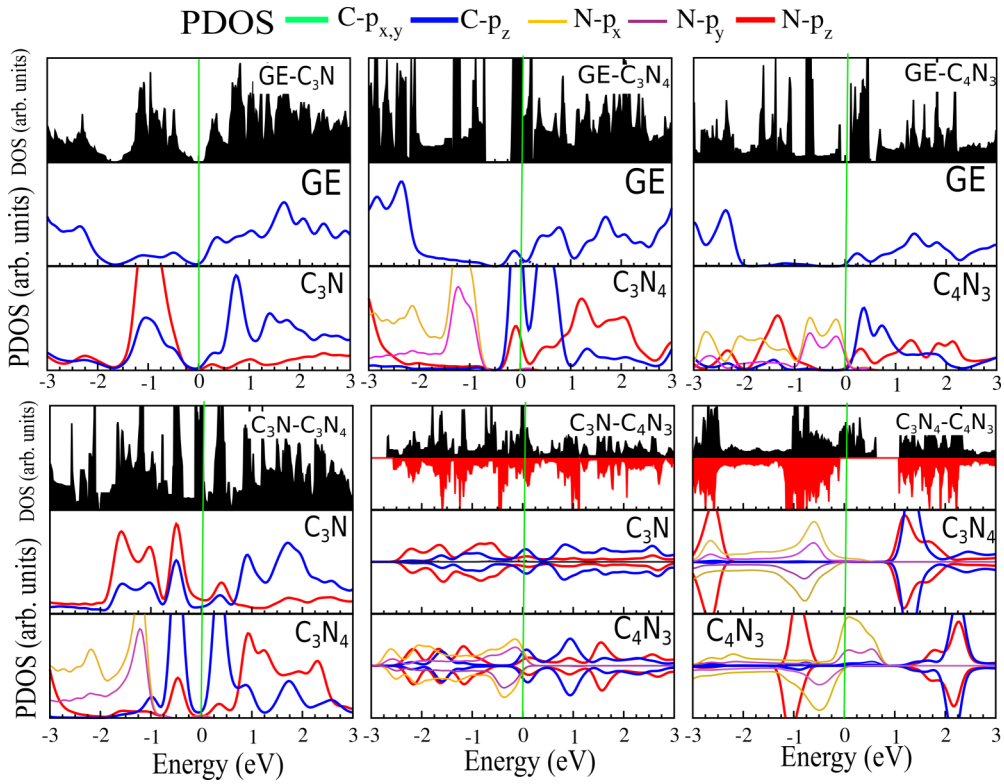

FIG. 6. (Color online.) The density of states and partial density of states of the studied HTJ.

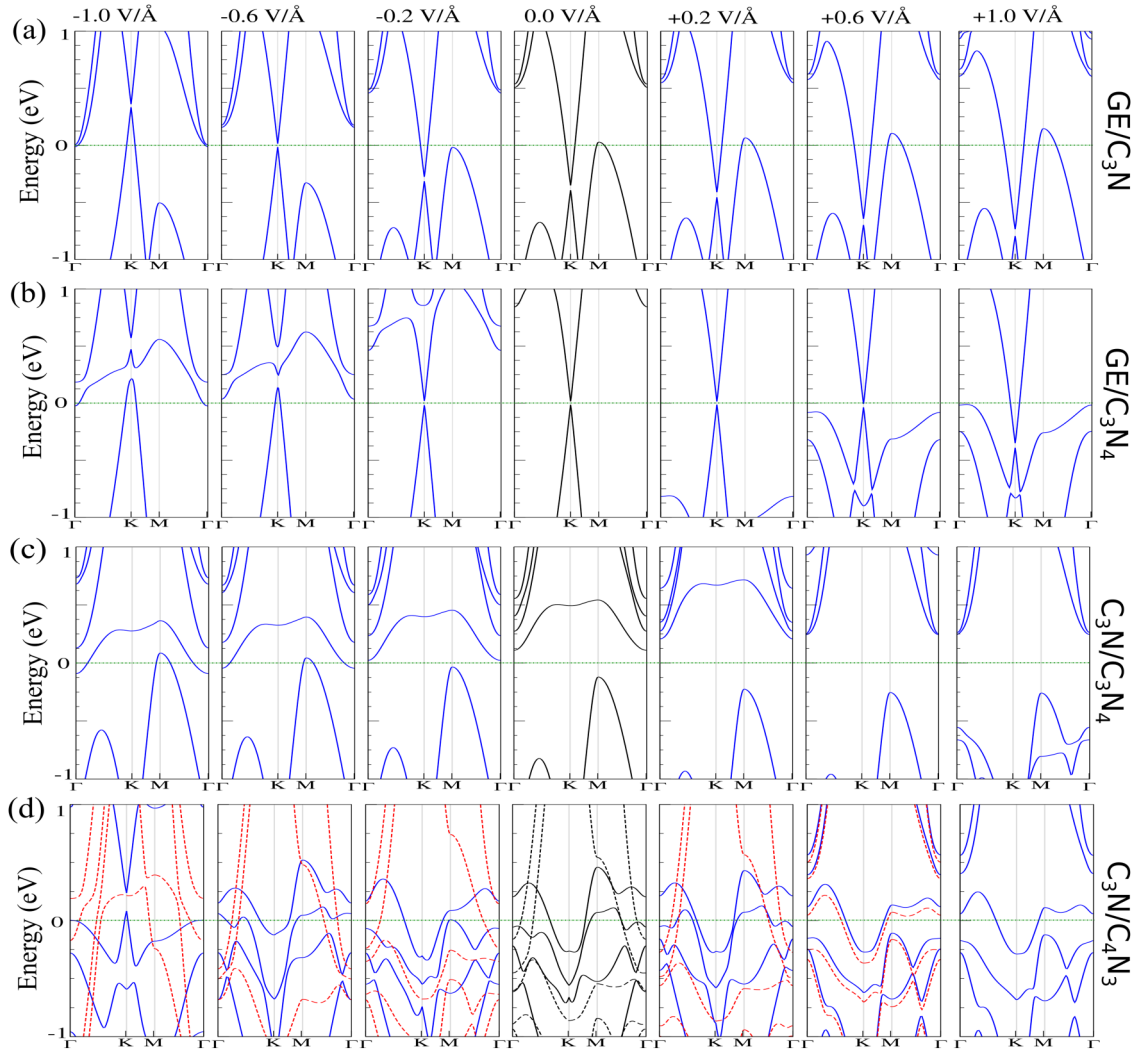

FIG. 7. The electronic band structure of (a) GE/C_3N, (b) GE/C_3N_4, (c) C_3N/C_3N_4, and (d) C_3N/C_4N_3 heterostructures with respect to the applied an electric field. The positive (negative) electric field denotes parallel (antiparallel) to the z axis. The zero of energy is set at the E_F.

Supplemental Material we depict the band structure of monolayer and corresponding bilayers.

D. Binding energy between two layers

The binding energy stored between the two layers of the HTSs (i.e., the adhesion energy) can be calculated by varying the interlayer distance between two layers. Additional calculations were done to obtain the energy variation for a given interlayer distance. We start from two optimized layers and perform energy calculations. Moving one layer with respect to the other in vertical direction yields binding energy profile. The results for two typical HTSs (GE/C_3N and C_3N/C_4N_3) are shown in Fig. 4. The minimum energy is set to zero, i.e., $\Delta E_n = E_n(z) - E_n(z_{\text{eq}})$ and the horizontal axis is shifted by z_{eq}, i.e., $\Delta z = z - z_{\text{eq}}$. The results show that the adhesion between GE and C_3N is stronger than that of between C_3N and C_4N_3. Therefore, exfoliating $C_{n'}N_{m'}/C_nN_m$ would be easier than that of GE/C_nN_m. As expected, for very large interlayer distances, the pristine graphene properties can be recovered. The binding energy profile between GE and g-C_3N_4 was reported by Li *et al.* [46].

IV. GE-GCN HETEROJUNCTIONS

By sticking GCN to GE laterally, we made six HTJs. The optimized atomic structures and corresponding electronic band structures of HTJs are shown in Figs. 4(a) and 4(b). The corresponding lattice parameters and electronic states of each HTJ are listed in Table III.

We found that the GE-C_3N and GE-C_4N_3 are direct semiconductors with narrow band gaps of 150 meV and 100 eV, respectively. By analyzing the charge distribution along the contact line between GE and C_nN_ms, we noticed that there is a minimum change in the charge distribution on the contact line of GE-C_3N (in Fig. S3, we depict valance charge density distribution over the studied HTJs, see Supplemental Material Fig. S3). The semiconducting properties of GE-C_3N and minimal mismatch at the contact line makes GE-C_3N an exceptional HTJ that may be realized for potential applications.

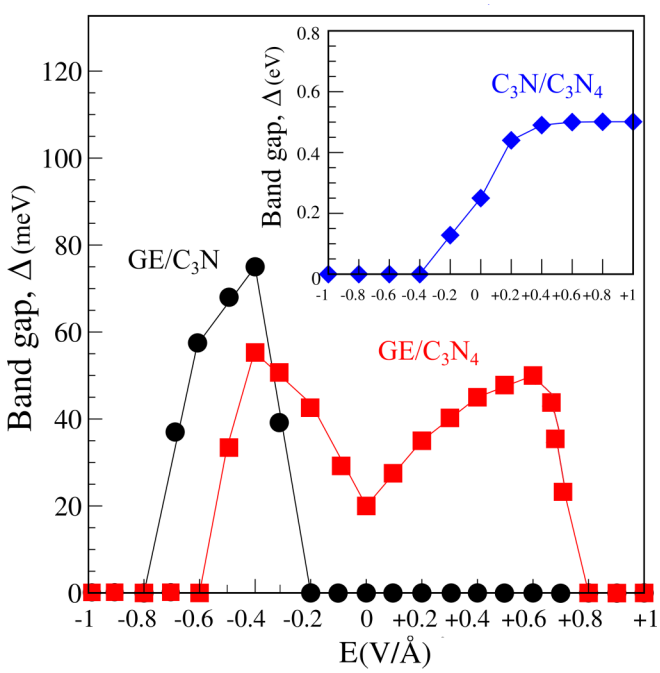

FIG. 8. The variation of band gap with perpendicular electric field for three HTSs.

On the other hand, the electronic structure of GE-C_3N_4 results in a semimetal nodal-line characteristic having a nodal line around the K point. The latter is related to crossing of the energy bands of VBM and CBM at two points along the Fermi level. Generally, in nodal line materials, the Dirac-like crossings along special lines in momentum space create either a closed ring or line of degeneracies, rather than discrete points [see two arrows in Fig. 5(b)]. The appearance of the nodal line in GE-C_3N_4 originates from the p_z orbitals of both C and N (see Fig. 6). We found semiconducting characteristics with a band gap of 80 meV at the M point for C_3N-C_3N_4. Furthermore, C_3N-C_4N_3 becomes a ferromagnetic metal having a magnetic moment of 4 μ_B. The C_3N_4-C_4N_3 HTJ shows a half-metal characteristic, where only spin-up states crossing the Fermi level and the spin-down channel has band gap. The band split induces a magnetic moment of about $1.7\mu_B$.

From the DOS and PDOS of C_3N-C_3N_4 (see Fig. 6), we found that VBM mainly belongs to the N-$p_{x,y}$ and N/C-p_z orbitals, while the CBM originates from the C-p_z orbitals. The state of C_3N-C_4N_3, at E_F belongs to the C-p_z orbitals in both ↑ and ↓ spin channels. The latter confirms the metallic characteristics and also the magnetism nature of the system, which has a magnetic moment of 1.7 μ_B. Finally, the C_3N_4-C_4N_3 exhibits half-metal characteristics. The metallic behavior belongs to the N-$p_{x,y}$ orbitals in ↑ spin channel.

The summary of the electronic state of the studied HTJ and corresponding transition states are listed in Table II. The results of this section are helpful for designing functional materials such as those proposed recently by Liu *et al.* [1].

V. EFFECTS OF PERPENDICULAR ELECTRIC FIELD

We turn our attention to the effects of perpendicular electric field on the electronic properties of HTSs. The variation of the electronic band structure of four studied HTSs with respect to the electric field (E) is shown in Fig. 7. The positive direction of the electric field is along the z axis, see Fig. 2(a). By calculating the electronic band structure of four HTSs (GE/C_3N, GE/C_3N_4, C_3N/C_3N_4, and C_3N/C_4N_3), different effects are obtained which are as follows:

(1) Although in the absence of electric field GE/C_3N is a metal, it becomes a semiconductor with direct band gap in the presence of electric fields in the range $E = (-0.4, -0.6)$ V/Å. Interestingly, the metallically of GE/C_3N is preserved in the presence of positive electric fields.

(2) The GE/C_3N_4 is a direct semiconductor having band gap of 20 meV. Our results show that by increasing $|E|$ up to 0.4V/Å, the band gap increases almost linearly. The larger $|E|$ ($E > 0.6$ V/Å and $E < -0.4$ V/Å) causes fast decrease in the band gap, i.e., semiconductor-to-metal transition, see Fig. 8.

(3) The C_3N/C_3N_4 exhibit a indirect semiconductor with band gap of 250 meV when $E = 0$, but its band gap increases up to 450 meV when $E = 0.4$ V/Å and remains constant beyond that. Surprisingly, by reversing the electric fields direction completely different behavior happens, i.e., the band gap decreases to 60 meV when $E = -0.2$ V/Å and approaches zero beyond $E = -0.4$ V/Å. Therefore, for the electric fields $E < -0.4$ V/Å, i.e. a semiconductor-to-metal transition occurs, see the inset in Fig. 8.

(4) The C_3N/C_4N_3 is a metal with nonmagnetic ground state when $E = 0$. The metallicity is preserved for the electric fields between +0.2 and +0.8 V/Å. Under the field $E = +1$ V/Å, a metal to ferromagnetic-metal transition occurs and the system gains a magnetic moment of $0.3\mu_B$.

(5) We found an electronic state transition in the band structure of C_3N/C_4N_3 (metal to ferromagnetic metal) for the electric fields in the range −0.4 V/Å and −0.6 V/Å, together gaining a magnetic moments of 0.8 and 1.9 μ_B, respectively. Also it becomes a half metal when $E = -0.8$ V/Å, having a magnetic moment of $5\mu_B$ and Dirac half metal when E = −1.0 V/Å with a magnetic moment of $3\mu_B$.

VI. SUMMARY AND DISCUSSION

In summary, we systematically studied the structural and electronic properties of HTSs made of graphene and three graphitic carbon nitrides, i.e., C_3N, C_3N_4, and C_4N_3. We found that C_3N, C_3N_4 with planar structures are semiconductors while C_4N_3 exhibits half-metallic features with significant DOS at Fermi level. The half metallicity originates mainly from the $p_{x,y}$ planar orbitals of N atoms in C_4N_3 monolayer. We found that the hybridized systems made of C_4N_3 and GE or C_3N are ferromagnetic HTSs, while the bilayer made of C_4N_3 and C_3N_4 is metal.

For the GE-C_3N_4 HTJ, we found a nodal line feature which originates from the p_z orbitals of both C and N. Also, we found that C_3N_4-C_4N_3 and C_3N-C_4N_3 systems have nonzero magnetic moments with half-metallicity and ferromagnetic-metal characteristics, respectively. We also found that there is a minimum change in the charge distribution on the contact line of GE-C_3N. The valance charge distribution and the degree of porosity and its (the hollow sites in GCN)

in C_3N_4 and C_3N_4 significantly influence the electronic structure of GCN monolayers and corresponding HTSs and HTJs.

The electronic properties of the vdW HTSs were modulated by applying a perpendicular electric field. We found that in the presence of an electric field which is directed from GE to C_3N, i.e., $E \geqslant 0$, there is no band gap in the GE/C_3N but by reversing the direction of electric field for $E < -0.2$ V/Å, a band gap of about 40 meV is opened. Moreover, other similar asymmetrical effects were obtained for C_3N/C_3N_4. These asymmetrical effects cannot happen either in bilayer graphene (where only a band gap of 100 meV can be induced in the system independent of the direction of applied electric field) or in GE/g-C_3N_4 [46]. Depending on the direction of the applied electric field, these two HTSs show a metallic or semiconducting behavior. This might be promising for the realization of new HTSs that have electrically tunable band gaps and unusual responses to the applied electric field. This phenomena is of great significance for both basic physics and applications.

[1] X. Liu and M. C. Hersam, Sci. Adv. **5**, 6444 (2019).
[2] Y. Zheng, J. Liu, J. Liang, M. Jaroniec, and S. Qiao, Energy Environ. Sci. **5**, 6717 (2012).
[3] J. Mahmood, E. K. Lee, M. Jung, D. Shin, I.-Y. Jeon, S.-M. Jung, H.-J. Choi, J.-M. Seo, S.-Y. Bae, S.-D. Sohn, N. Park, J. H. Oh, H.-J. Shin, and J.-B. Baek, Nat. Commun. **6**, 6486 (2015).
[4] B. Mortazavi, Carbon **118**, 25 (2017).
[5] M. B. Tagani and S. I. Vishkayi, J. Appl. Phys. **124**, 8 (2018).
[6] G. Zhu, K. Lü, Q. Sun, Y. Kawazoe, and P. Jena, Comput. Mater. Sci. **81**, 275 (2014).
[7] X. Li, Sh. Zhang, and Q. Wang, Phys. Chem. Chem. Phys. **15**, 7142 (2013).
[8] A. J. Mannix, B. Kiraly, M. C. Hersam, and N. P. Guisinger, Nat. Rev. Chem. **1**, 0014 (2017).
[9] A. Du, S. Sanvito, and S. C. Smith, Phys. Rev. Lett. **108**, 197207 (2012).
[10] L. Britnell, R. M. Ribeiro, A. Eckmann, R. Jalil, B. D. Belle, A. Mishchenko, Y.-J. Kim, R. V. Gorbachev, T. Georgiou, S. V. Morozov, A. N. Grigorenko, A. K. Geim, C. Casiraghi, A. H. C. Neto, and K. S. Novoselov, Science **340**, 1311 (2013).
[11] H. Tian, Zh. Tan, C. Wu, X. Wang, M. A. Mohammad, D. Xie, Y. Yang, J. Wang, L.-J. Li, J. Xu, and T.-L. Ren, Sci. Rep. **4**, 5951 (2014).
[12] S. K. Singh, M. Neek-Amal, S. Costamagna, and F. M. Peeters, Phys. Rev. B **91**, 014101 (2014).
[13] C. R. Dean, A. F. Young, I. Meric, C. Lee, L. Wang, S. Sorgenfrei, K. Watanabe, T. Taniguchi, P. Kim, K. L. Shepard, and J. Hone, Nat. Nanotech. **5**, 722 (2010).
[14] X. Lin, Y. Xu, A. A. Hakro, T. Hasan, R. Hao, B. Zhang, and H. Chen, J. Mater. Chem. C **1**, 1618 (2013).
[15] J. Xue, J. Sanchez-Yamagishi, D. Bulmash, Ph. Jacquod, A. Deshpande, K. Watanabe, T. Taniguchi, P. Jarillo-Herrero, and B. J. LeRoy, Nat. Mater. **10**, 282 (2011).
[16] M. Neek-Amal, A. Sadeghi, G. R. Berdiyorov, and F. M. Peeters, Appl. Phys. Lett. **103**, 261904 (2013).
[17] Y. Cai, Ch.-P. Chuu, C. M. Wei, and M. Y. Chou, Phys. Rev. B **88**, 245408 (2013).
[18] Y. Sun, C. Li, Y. Xu, H. Bai, Z. Yao, and G. Shi, Chem. Commun. **46**, 4740 (2010).
[19] W. Hu, T. Wang, and J. Yang, J. Mater. Chem. C **3**, 4756 (2015).
[20] J. Wang, Zh. Guan, J. Huang, Q. Li, and J. Yang, J. Mater. Chem. A **2**, 7960 (2014).
[21] S. Ali Ansari, M. O. Ansari, and M. Hwan Cho, Sci. Rep. **6**, 27713 (2016).
[22] A. Hashmi and J. Hong, Sci. Rep. **4**, 4374 (2014).
[23] A. Bafekry, S. Farjami Shayesteh, and F. M. Peeters, Phys. Chem. C **123**, 12485 (2019).
[24] A. Bafekry, M. Ghergherehchi, and S. Farjami Shayesteh, Phys. Chem. Chem. Phys. **21**, 10552 (2019).
[25] A. Bafekry, C. Stampfl, S. Farjami Shayesteh, and F. M. Peeters, Adv. Elec. Mater. **5**, 1900459 (2019).
[26] A. Bafekry, S. Farjami Shayesteh, and F. M. Peeters, Phys. Chem. Chem. Phys. **21**, 21070 (2019).
[27] Sh. Guan, Y. Cheng, Ch. Liu, J. Han, Y. Lu, A. Y. Shengyuan, and Y. Yao, Appl. Phys. Lett. **107**, 231904 (2015).
[28] A. Bafekry, M. Ghergherehchi, S. Farjami Shayesteh, and F. M. Peeters, Appl. Phys. **126**, 144304 (2019).
[29] A. Bafekry, B. Mortazavi, and S. Farjami Shayesteh, J. Magn. Magn. Mater., **491**, 165565 (2019).
[30] S. K. Singh, M. Neek-Amal, and F. M. Peeters, J. Chem. Phys. **140**, 074304 (2014).
[31] M. Neek-Amal, J. Beheshtian, A. Sadeghi, K. H. Michel, and F. M. Peeters, J. Phys. Chem. C **117**, 13261 (2013).
[32] J. Beheshtian, A. Sadeghi, M. Neek-Amal, K. H. Michel, and F. M. Peeters, Phys. Rev. B **86**, 195433 (2012).
[33] A. Bafekry, C. Stampfl, M. Ghergherehchi, S. Farjami Shayesteh, Carbon **157**, 371 (2020).
[34] A. Bafekry, B. Akgenc, S. F. Shayesteh, B. Mortazavi, Appl. Surf. Sci. **505**, 144450 (2020).
[35] J. P. Perdew, K. Burke, and M. Ernzerhof, Phys. Rev. Lett. **77**, 3865 (1996).
[36] T. Ozaki, Phys. Rev. B **67**, 155108 (2003).
[37] N. Troullier and J. L. Martins, Phys. Rev. B **43**, 1993 (1991).
[38] T. Ozaki and H. Kino, Phys. Rev. B **69**, 195113 (2004).
[39] H. J. Monkhorst and J. D. Pack, Phys. Rev. B **13**, 5188 (1976).
[40] T. Bučko, J. Hafner, S. Lebègue, and J. G. Angyán, J. Phys. Chem. A **114**, 11814 (2010).
[41] See Supplemental Material at http://link.aps.org/supplemental/10.1103/PhysRevB.101.085417 for more details about structural and electronic properties of single layer of graphene-graphitic carbon nitride, which includes Refs. [7,22,43,46–54].
[42] M. Neek-Amal and F. M. Peeters, Appl. Phys. Lett. **104**, 041909 (2014).
[43] A. K. Geim and K. S. Novoselov, Nat. Mater. **6**, 183 (2007).
[44] J. D. Correa and E. Cisternas, Solid State Commun. **241**, 1 (2016).
[45] K. Zollner, M. Gmitra, and J. Fabian, Phys. Rev. B **99**, 125151 (2019).

[46] X. Li, Y. Dai, Y. Ma, S. Hana, and B. Huanga, Phys. Chem. Chem. Phys. **16**, 4230 (2014).

[47] J. Mahmood, E. K. Lee, M. Jung, D. Shin, H.-J. Choi, J.-M. Seo, S.-M. Jung, D. Kim, F. Li, M. S. Lah, N. Park, H.-J. Shin, J. H. Oh, and J.-B. Baek, Proc. Natl. Acad. Sci. USA, **113**, 7414 (2016).

[48] S. Mizuno and M. Fujita, and K. Nakao, Synth. Met. **71**, 1869 (1995).

[49] E. Kroke, M. Schwarz, E. Horath-Bordon, P. Kroll, B. Noll, and A. D. Norman, Sci. Rep. **4**, 4374 (2015).

[50] X. Zhang, M. Zhao, A. Wang, X. Wang, and A. Du, J. Mater. Chem. C **1**, 6265 (2013).

[51] H. Wu, Y. Liu, E. Kan, Y. Ma, W. Xu, J. Li, M. Yan, R. Lu, J. Wei, and Y. Qian, J. Phys. D: Appl. Phys. **49**, 295301 (2016).

[52] P. Giannozzi, S. Baroni, N. Bonini, M. Calandra, R. Car, C. Cavazzoni, D. Ceresoli, G. L. Chiarotti, M. Cococcioni, I. Dabo *et al.*, J. Phys.: Condens. Matter **21**, 395502 (2009).

[53] Q. Hu, Q. Wu, H. Wang, J. He, and G. Zhang, Phys. Status Solidi B **249**, 784 (2011).

[54] H. J. Xiang, B. Huang, Z. Y. Li, S.-H. Wei, J. L. Yang, and X. G. Gong, Phys. Rev. X **2**, 011003 (2012).